POLARIZATION AND PYROELECTRIC COEFFICIENTS OF ANTIFERRODISTORTIVE BOUNDARIES: $SrTiO_3$ AS AN EXAMPLE

J.V. JAKOVENKO,[1,2] E.A. ELISEEV,[3] S.V. SVECHNIKOV,[2] A.N. MOROZOVSKA[4]

[1]Taras Shevchenko National University of Kyiv, Faculty of Physics
(Bld. 1, 2, Prosp. Academician Glushkov, Kyiv 03187, Ukraine)

[2]V.E. Lashkaryov Institute of Semiconductor Physics, Nat. Acad. of Sci. of Ukraine
(41, Prosp. Nauky, Kyiv 03028, Ukraine)

[3]I.M. Frantsevich Institute for Problems of Materials Science, Nat. Acad. of Sci. of Ukraine
(3, Krzhyzhanivskyi Str., Kyiv 03142, Ukraine)

[4]Institute of Physics, Nat. Acad. of Sci. of Ukraine
(46, Prosp. Nauky, Kyiv 03680, Ukraine)

PACS 77.22.Ej, 77.70.+a

The spatial distributions and the temperature dependences of a local polarization and the pyroelectric coefficient in a vicinity of antiferrodistortive boundaries in $SrTiO_3$ at temperatures lower than that of the antiferrodistortive structural phase transition ($\approx$ 105 K) have been studied analytically and numerically in the framework of the Landau–Ginsburg–Devonshire theory. The polarization in the near-wall region is supposed to emerge as a result of the flexoelectric field and the rotostriction.

1. Introduction

Considerable attention of researchers is attracted by unique properties of perovskite oxide surfaces. In their subsurface layers, a 2-dimensional gas of collectivized electrons, the related 2-dimensional superconductivity [1–3], charged domain walls [4], magnetism [5, 6], and multiferroic properties [7,8] were observed. Near-surface regions, by their nature, are characterized by the gradients of order parameters such as the spontaneous deformation, oxygen octahedral rotations, polarization, and spin. These order parameters can be strongly coupled by means of the equation of state, which induces new phenomena absent from corresponding bulk materials.

In near-surface layers of perovskite oxides with antiferrodistortive phase transitions, the strain gradients, u_{ij}, and the gradients of tilt angles of oxygen octahedra (O_6-octahedra) characterized by the axial vector Φ_i ($i = 1, 2, 3$) [9] take place. As a consequence, the near-surface layers reveal the phenomena of flexoelectric effect (i.e. the emergence of a polarization proportional to the deformation gradient) and rotostriction (i.e. the square-law dependence between the rotation of octahedra and the elastic strain). The relation between those phenomena can lead to the ferroelectric polarization in a region, where the gradient of tilt angles for oxygen octahedra differs from zero. Earlier, it was predicted that the vector of spontaneous polarization regarded as a secondary order parameter can appear in a ferroelastic domain wall owing to the biquadratic coupling $\eta_{ijkl} P_i P_j \Phi_k \Phi_l$ [10]. In the framework of the Landau–Ginsburg–Devonshire (LGD) theory and by carrying out a numerical simulation by the molecular dynamics technique, it was shown that this term induces the polarization of ferroelastic domain walls in $CaTiO_3$ [12]. Recently, Salje *et al.* [13] observed the ferrielectric polarization in a vicinity of the ferroelastic domain walls in $CaTiO_3$ at room temperature, by using transmission electron microscopy with an atomic resolution. Zubko *et al.* [14] experimentally observed strong variations for the coefficient of direct flexoelectric effect in $SrTiO_3$ below the temperature of the antiferrodistortive structural phase transition ($T_S \approx$105 K)

and considered that this effect can probably be induced by the polarization that emerges in a vicinity of domain walls between elastic twins.

Flexoelectric coupling, which exists in all materials and is rather strong in many perovskites [14–18], should result in the appearance of a spontaneous polarization in ferroelastic domain walls of non-ferroelectric perovskites. The appearance of the polarization induced by the flexoeffect in a vicinity of antiferrodistortive phase boundaries (APBs) has not been studied analytically. This fact stimulated us to carry out analytical and numerical calculations on the basis of an LGD-expansion of the free energy density in order to examine the influence of the flexoelectric coupling on the spontaneous polarization and the pyroelectric coefficient near APBs in non-ferroelectric perovskites (with tilted O_6-octahedra), by using $SrTiO_3$ as an example.

2. Basic Equations

Let us analyze the energy of domain walls using the free energy functional, which corresponds to a prototype phase of perovskite for the polar and structural order parameters, the latter being the tilt angle for O_6-octahedra. In the prototype phase at a temperature above that of structural phase transition, when there are no angle of spontaneous octahedron rotation and no spontaneous polarization, the free energy density looks like [23]:

$$F_d = \frac{a_i(T)}{2}P_i^2 + \frac{a_{ijkl}}{4}P_iP_jP_kP_l + \ldots + \frac{1}{2}g_{ijkl}\times$$

$$\times\left(\frac{\partial P_i}{\partial x_j}\frac{\partial P_k}{\partial x_l}\right) - P_i\frac{E_i^d}{2} + q_{ijkl}u_{ij}P_kP_l +$$

$$+\frac{c_{ijkl}}{2}u_{ij}u_{kl} + r_{ijkl}^{(\Phi)}\Phi_k\Phi_l u_{ij} + \frac{f_{ijkl}}{2}\times$$

$$\times\left(\frac{\partial P_k}{\partial x_l}u_{ij} - P_k\frac{\partial u_{ij}}{\partial x_l}\right) +$$

$$+\frac{b_i}{2}\Phi_i^2 + \frac{b_{ij}}{4}\Phi_i^2\Phi_j^2 + \frac{b_{ijk}}{6}\Phi_i^2\Phi_j^2\Phi_k^2 +$$

$$+\frac{\eta_{ijkl}}{2}P_iP_j\Phi_k\Phi_l + \frac{v_{ijkl}}{2}\left(\frac{\partial\Phi_i}{\partial x_j}\frac{\partial\Phi_k}{\partial x_l}\right), \quad (1)$$

where Φ_i are the components of the structural order parameter (the axial vector of tilt angle for O_6-octahedra, which is determined by the displacements of oxygen atoms in the structural phase); and $u_{ij}(\mathbf{x})$ is the strain tensor. The summation is carried out over the repeated indices. The temperature dependences of the coefficients

$$a_i(T) = \alpha_T T_q^{(E)}\left(\coth\left(T_q^{(E)}/T\right) - \coth\left(T_q^{(E)}/T_0^{(E)}\right)\right)$$

and

$$b_i(T) = \beta_T T_q^{(\Phi)}\left(\coth\left(T_q^{(\Phi)}/T\right) - \coth\left(T_q^{(\Phi)}/T_S\right)\right)$$

are described by the Barrett law for quantum paraelectrics [19–21]. The quadratic terms composed of the tensors of gradient coefficients g_{ijkl} and v_{ijkl}, respectively, are positive definite; f_{ijkl} is the fourth-rank tensor of flexoelectric coupling; q_{ijkl} is the fourth-rank electrostriction tensor; and $r_{ijkl}^{(\Phi)}$ is the rotostriction tensor. The biquadratic connection between the components of a tilt angle, Φ_i, and the polarization, P_i, is determined in terms of the constants η_{ijkl}. The flexoelectric effect tensor f_{ijkl} and the rotostriction tensor $r_{ijkl}^{(\Phi)}$ have nonzero components in all phases and for any symmetry of the system. The quantities E_i^d are the components of electric depolarization field, if any; the external field is supposed to be absent. The distribution of the polarization components $P_i(x_i)$ generates a depolarization field in the wall [22],

$$E_i^d(x_i) = -\frac{1}{\varepsilon_0\varepsilon_b}P_i(x_i). \quad (2)$$

Here, i=1, 3, and $\varepsilon_0\varepsilon_b$ is the dielectric permittivity of the lattice. The depolarization field $E_i^d(x_i)$ strongly reduces the polarization component $P_i(x_i)$.

The Euler–Lagrange equations of state are derived by minimizing the free energy,

$$\frac{\partial F_b}{\partial\Phi_i} - \frac{\partial}{\partial x_j}\left(\frac{\partial F_b}{\partial\left(\partial\Phi_i/\partial x_j\right)}\right) = 0, \quad (3a)$$

$$\frac{\partial F_b}{\partial P_i} - \frac{\partial}{\partial x_j}\left(\frac{\partial F_b}{\partial\left(\partial P_i/\partial x_j\right)}\right) = 0, \quad (3b)$$

$$\frac{\partial F_b}{\partial u_{ij}} - \frac{\partial}{\partial x_k}\left(\frac{\partial F_b}{\partial\left(\partial u_{ij}/\partial x_k\right)}\right) = \sigma_{ij}. \quad (3c)$$

On the right-hand side of Eq. (3c), the tensor of mechanical stresses $\sigma_{ij}(\mathbf{x})$ is introduced. It satisfies three equations of mechanical equilibrium,

$$\partial\sigma_{ij}(\mathbf{x})/\partial x_j = 0. \quad (3d)$$

The explicit form of the equations of state is given in works [23, 24]. In the phase with relatively tilted oxygen octahedra, the strains $u_{ij}(\mathbf{x})$ look like

$$u_{mn}(\mathbf{x}) = s_{mnij}\,\sigma_{ij} - 2R^{(\Phi)}_{mnkl}\Phi_k\Phi_l - \\ - F_{mnkl}\frac{\partial P_k}{\partial x_l} - Q_{mnkl}P_kP_l, \qquad (4)$$

where s_{mnij} is the elastic stiffness tensor, $R^{(\Phi)}_{ijkl} = s_{ijmn}r^{(\Phi)}_{mnkl}$ is the rotostriction deformation tensor, $Q_{ijkl} = s_{ijmn}q_{mnkl}$ is the electrostriction deformation tensor, and $F_{ijkl} = s_{ijmn}f_{mnkl}$ is the flexoelectric deformation tensor. The substitution of those expressions for mechanical stresses into Eq. (3c) brings about a closed system of equations for the components of the polarization vector and the structural order parameter.

3. Contribution of Flexo-Rotational Effect to Near-Wall Polarization and Pyroelectric Coefficient

In the structural bulk phase of $SrTiO_3$ with relatively tilted O_6-octahedra, which is stable at temperatures $T < T_S$, one component of the spontaneous structural order parameter, $\Phi^S_3(\mathbf{x})$, appears. The other components, Φ_1 and Φ_2, can differ from zero in vicinities of various elastic domain walls.

3.1. Manifestations of flexo-rotational effect on antiferrodistortive phase boundaries

Antiferrodistortive phase boundaries (APBs) are classed into "soft" and "hard" ones [22], which differ from each other by the magnitude of intrinsic energy of a domain wall that is necessary for its formation. Soft APBs possess a substantially lower energy than hard ones. The existence of boundaries of both types is governed not only by the energy balance, but sooner by spatial restrictions (the boundary shape), as well as the nature of external factors. The flexoelectric effect can induce the polarization of APBs in the whole structural phase [23], which agrees with experiment [14].

"Soft" APBs with $\Phi_3(x_3) \neq 0$, $\Phi_2 \equiv 0$, and $\Phi_3 \equiv 0$ induce nonzero polarization distributions $P_3(x_3)$, which are of either the even or odd type functionally, whereas $P_1 \equiv 0$ and $P_2 \equiv 0$ (see Fig. 1). The case of soft APBs is the most suitable for obtaining an analytical solution, even if it would be approximate. The sign of the flexoelectric coefficient is responsible for the appearance of head-to-head or tail-to-tail P_3-odd distributions

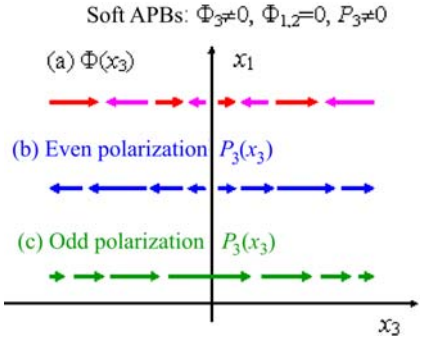

Fig. 1. Schematic distribution of the structural order parameter, $\Phi_3(x_3)$, and the polarization, $P_3(x_3)$, near the APB [23]

of polarization. Therefore for $SrTiO_3$ with a positive F_{12}-value, only soft head-to-head P_3-odd distributions are realized. Despite that the odd distribution is more beneficial energetically [23], the matter concerns the experimental observation of the odd polarization distribution in and the pyroelectric response of the near-wall region, because the averaged polarization equals zero in this case. The application of transmission electron microscopy (TEM) allows the picometer resolution to be achieved and a spontaneous polarization in vicinities of ferroelastic twin domain boundaries to be observed [13]. Curves *e-f* in Fig. 2 in work [13] demonstrate the features of even polarization distributions on elastic twins in $CaTiO_3$. Therefore, we hope that the local spontaneous polarization of elastic domain walls can reliably be observed in ferroelastics $CaTiO_3$, $SrTiO_3$, and $EuTiO_3$ with the use of TEM.

The spatial distribution of the pyroelectric coefficient (the local pyroelectric response) was measured directly using the pyroelectric scanning probe microscopy (PyroSPM) method with a resolution of 50 nm [25]. Similarly to the conventional piezoelectric power microscopy, where the transverse resolution is at least 2 to 5 times better than the sizes determined by effective probe dimensions (see, e.g., Fig. 12 in work [26]), the resolution of PyroSPM is determined, first of all, by the curvature radius of a probe tip. Therefore, the scanning using a probe with a tip curvature radius of 5–10 nm [27] allows the local piezoresponse to be registered with a transverse resolution of 2–5 nm (see, e.g., works [27, 28] and references therein). Hence, by applying a probe 5 nm in dimension, it is possible to measure the local pyroelectric response with a resolution of about 2–5 nm. Below, we calculate the maximum and average values of pyroelectric coefficient.

For the case of soft APBs (the solution depends on x_3), it is possible to obtain an expression for the field

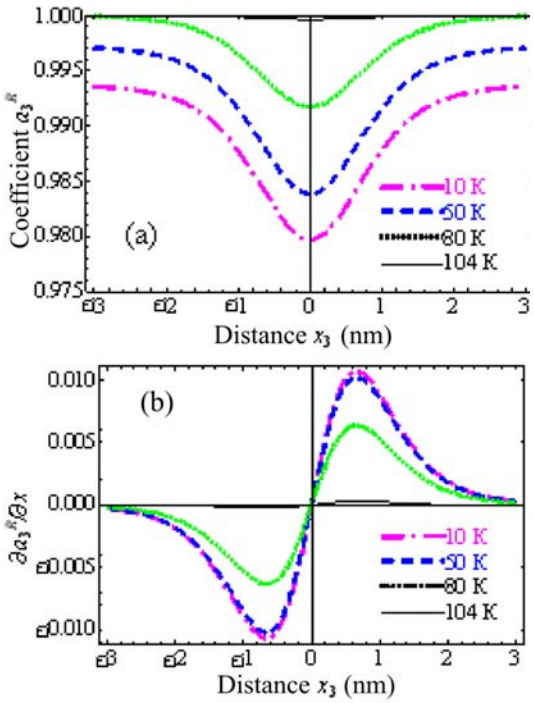

Fig. 2. Spatial distributions of (a) the coefficient a_3^R normalized by its maximum value and (b) its derivative with respect to the coordinate at various temperatures

of mechanical stresses, which satisfies the equation of mechanical balance (3d) and looks like

$$\sigma_{11}(x_3) = \sigma_{22}(x_3) = \frac{U(x_3)}{s_{11}+s_{12}}. \tag{5}$$

Provided that

$$\sigma_{33} = \sigma_{13} = \sigma_{12} = \sigma_{23} = 0, \tag{6}$$

$$U(x_3) = R_{12}^{(\Phi)}\left(\left(\Phi_3^S\right)^2 - \Phi_3^2\right) - \left(Q_{12}P_3^2 - F_{12}\frac{\partial P_3}{\partial x_3}\right). \tag{7}$$

Under condition (6), Eq. (3d) gives rise to a closed system of equations for the polarization component and the tilt angle of O_6-octahedra,

$$2\left(b_1 - \eta_{11}P_3^2 - \frac{2R_{12}^{(\Phi)}U}{s_{11}+s_{12}}\right)\Phi_3 + 4b_{11}\Phi_3^3 - v_{11}\frac{\partial^2\Phi_3}{\partial x_3^2} = 0, \tag{8a}$$

$$2\left(a_1 - \eta_{11}\Phi_3^2 - \frac{2Q_{12}U}{s_{11}+s_{12}}\right)P_3 + 4a_{11}P_3^3 - g_{11}\frac{\partial^2 P_3}{\partial x_3^2} = E_3^{\text{ext}} + E_3^d + \frac{2F_{12}}{s_{11}+s_{12}}\frac{\partial U}{\partial x_3}. \tag{8b}$$

The boundary conditions for the component of the axial vector are $\Phi_3(x_3 \to \pm\infty) = \pm\Phi_3^S$ and $\Phi_3(x_3 = 0) = 0$, where $\Phi_3^S = \sqrt{-b_1(T)/(2b_{11})}$ is the component of a spontaneous tilt angle in the monodomain state with mutually tilted O_6-octahedra. The boundary conditions for the polarization are $P_3(x_3 \to \pm\infty) = 0$ and $P_3(0) = 0$ (the odd solution). The depolarization field is $E_3^d(x_3) = -P_3(x_3)/(\varepsilon_0\varepsilon_b)$, and the external field is absent.

In the first order of perturbation theory with respect to a small polarization, we arrive at a simplified form of system (8),

$$2\left(b_1^- - \frac{2\left(R_{12}^{(\Phi)}\right)^2\Phi_S^2}{s_{11}+s_{12}}\right)\Phi_3 + 4\left(b_{11} + \frac{\left(R_{12}^{(\Phi)}\right)^2}{s_{11}+s_{12}}\right)\Phi_3^3 - v_{11}\frac{\partial^2\Phi_3}{\partial x_3^2} = 0, \tag{9a}$$

$$2a_3^R P_3 + 4a_{11}P_3^3 - \left(g_{11} + \frac{2F_{12}^2}{s_{11}+s_{12}}\right)\frac{\partial^2 P_3}{\partial x_3^2} = -\frac{2F_{12}R_{12}^{(\Phi)}}{s_{11}+s_{12}}\frac{\partial\Phi_3^2}{\partial x_3}. \tag{9b}$$

Here, the coefficient

$$a_3^R = a_1 + 1/(\varepsilon_0\varepsilon_b) - \eta_{11}\Phi_3^2 - 2Q_{12}R_{12}^{(\Phi)}\left(\left(\Phi_3^S\right)^2 - \Phi_3^2\right)\Big/(s_{11}+s_{12}) \approx a_1 + 1/(\varepsilon_0\varepsilon_b). \tag{10}$$

From Fig. 2, one can see that the coefficient a_3^R is practically independent of the coordinate. In particular, its deviation from the value far from the wall does not exceed 3% and rather weakly depends on the temperature. Therefore, the derivative of a_3^R with respect to the coordinate can be neglected even in a very close vicinity to the domain wall.

After Eq. (9a) has been rewritten in a compact form,

$$4b_{11}\left(-\Phi_S^2\Phi_3 + \Phi_3^3\right) + \frac{4\left(R_{12}^{(\Phi)}\right)^2\left(\Phi_3^2 - \Phi_S^2\right)}{s_{11}+s_{12}}\Phi_3 - v_{11}\frac{\partial^2\Phi_3}{\partial x_3^2} = 0,$$

one can see that the dependence of the component Φ_3 of the structural order parameter, which characterizes the tilt angle of O_6-octahedra, can be approximated well by the formula

$$\Phi_3(x_3) = \Phi_S \tanh(x_3/l_\Phi), \tag{11}$$

where

$$l_\Phi(T) = \sqrt{-v_{11}\Big/\left(b_1(T)\left(1+\frac{\left(R_{12}^{(\Phi)}\right)^2}{(s_{11}+s_{12})\,b_{11}}\right)\right)}$$

is the correlation length. The distribution $\Phi_3(x_3)$ weakly depends on the polarization P_3, whereas the latter strongly depends on the vector of octahedron tilt angle and changes proportionally to the flexo-rotational field that appears on the right-hand side of Eq. (9b). The flexo-rotational field looks like

$$E_3^{\mathrm{FR}}(x_3) = -\frac{2F_{12}R_{12}^{(\Phi)}}{s_{11}+s_{12}}\frac{\partial\Phi_3^2}{\partial x_3} \approx$$

$$\approx -\frac{4F_{12}R_{12}^{(\Phi)}\Phi_S^2}{s_{11}+s_{12}}\frac{\sinh(x_3/l_\Phi)}{l_\Phi\cosh^3(x_3/l_\Phi)}. \tag{12}$$

Therefore, $E_3^{\mathrm{FR}}(x_3)$ is an odd function of x_3. Hence, Eq. (9b) reads

$$2a_3^R P_3 + 4a_{11}P_3^3 - g_{11}^R\frac{\partial^2 P_3}{\partial x_3^2} =$$

$$= -\frac{4F_{12}R_{12}^{(\Phi)}\Phi_S^2}{s_{11}+s_{12}}\frac{\sinh(x_3/l_\Phi)}{l_\Phi\cosh^3(x_3/l_\Phi)}. \tag{13}$$

Flexoelectric coupling also gives rise to a renormalization of the coefficient g_{11}^R in the gradient term in Eq. (13) to the form $g_{11}^R = \left(g_{11} + 2F_{12}^2/(s_{11}+s_{12})\right)$.

A very important fact for the further discussion is that the trivial solution $P_3 \equiv 0$ does not exist in vicinities of APBs because of the presence of a nonzero flexo-rotational field, $E_3^{\mathrm{FR}} \neq 0$. The components of the polarization P_3, which are perpendicular to the APB plane, are induced only by the flexo-rotational field E_3^{FR}. If $a_3^R > 0$, a "true ferroelectricity" is absent, i.e. there is no polarization hysteresis in the external field E_3^{ext}, but the pyroelectric coefficient $\Pi_3 = dP_3/dT$ should differ from zero, because the polarization component is temperature-dependent.

The trial polarization function looks like

$$P_3 = P_S p_0 \frac{\sinh(x_3/l_\Phi)}{\cosh^3(x_3/l_\Phi)} \tag{14}$$

and satisfies the boundary conditions $P_3(x_3 \to \pm\infty) = 0$ and $P_3(0) = 0$. In Eq. (14), the characteristic polarization $P_S = \sqrt{a_3^R/a_{11}}$, and p_0 is the dimensionless variational amplitude, which can be found by minimizing the free energy functional

$$F = \int_{-\infty}^{\infty} dx_3 \left(a_3^R P_3^2 + a_{11}P_3^4 + \frac{1}{2}\left(g_{11} + \frac{2F_{12}^2}{s_{11}+s_{12}}\right)\times\right.$$

$$\left.\times\left(\frac{\partial P_3}{\partial x_3}\right)^2 - E_3^{\mathrm{FR}}(x_3)\,P_3\right). \tag{15}$$

Neglecting the nonlinear term $a_{11}P_3^4$, we obtain

$$p_0(T) = \frac{14F_{12}R_{12}^{(\Phi)}\Phi_S^2}{P_S l_\Phi\left(20F_{12}^2 l_\Phi^2 + \left(10g_{11}l_\Phi^2 + 7a_3^R\right)(s_{11}+s_{12})\right)} \sim$$

$$\sim -\frac{2F_{12}R_{12}^{(\Phi)}\Phi_S^2}{P_S a_3^R l_\Phi(s_{11}+s_{12})}. \tag{16}$$

One can see that the polarization is absent in the absence of a flexoelectric field, because the biquadratic coupling induces no polarization in this case. The polarization amplitude decreases with the growth of the temperature. At the same time, the profile shape remains invariable.

In Fig. 3, the dependences of the polarization, $P_3(x_3)$, and the pyroelectric coefficient, $\Pi_3(x_3,T) = \frac{\partial P_3(x_3,T)}{\partial T}$, on the distance from the APB are plotted for various temperatures. From those dependences, one can see that the polarization falls down practically to zero at distances of 1 nm from the APB, whereas the pyroelectric coefficient vanishes at distances larger than 3 nm. The polarization maximum decreases as the temperature grows, owing to a reduction of the structural order parameter Φ_S^2. Accordingly, the pyroelectric coefficient grows at first, attains the maximum value at temperatures of about 80 K, and then decreases. In Appendix B, in the framework of approximate calculations, we obtained that the maximum of the pyroelectric coefficient for $SrTiO_3$ is observed at a temperature of $0.58T_q^{(\Phi)} = 84.1$ K.

The polarization is localized in a constant interval near the APB. At the same time, the localization interval for the pyroelectric coefficient increases with the

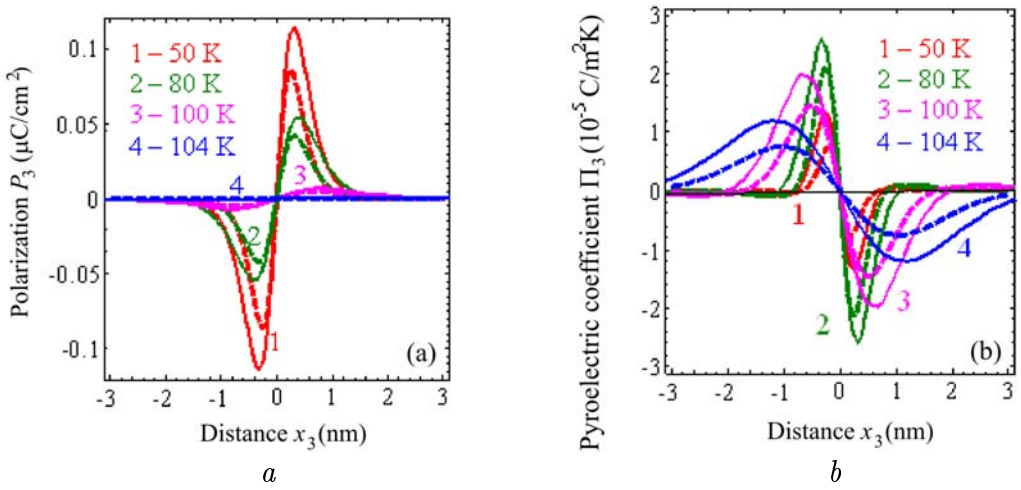

a *b*

Fig. 3. Analytical (solid curves) and numerical (dashed curves) spatial distributions of (*a*) the polarization component P_3 and (*b*) the pyroelectric coefficient Π_3 at various temperatures

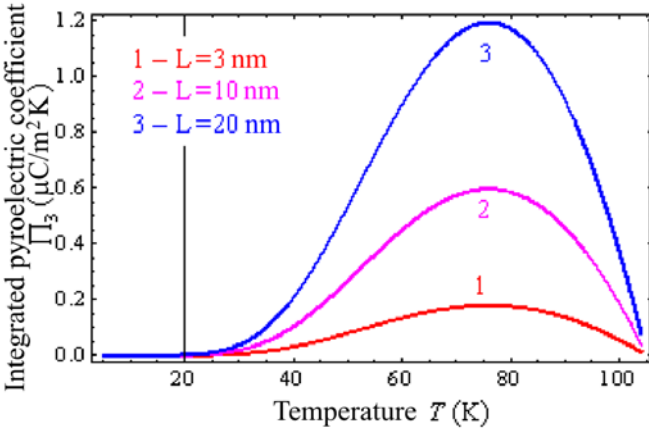

Fig. 4. Dependences of the integrated pyroelectric coefficient on the temperature at various averaging intervals L

temperature. Below 50 K, the polarization becomes temperature-independent, and the pyroelectric coefficient tends to zero.

In the analytical solution, the amplitudes of both the pyroelectric coefficient and the polarization are smaller than the corresponding values obtained numerically. In addition, the positions of the polarization and pyroelectric coefficient maxima calculated analytically are shifted toward the APB in comparison with the numerical results.

The integrated pyroelectric coefficient has a maximum at a temperature of 70 K and falls down when approaching the temperature of the structural phase transition and at temperatures below 30 K. The maximum value of integrated pyroelectric coefficient increases with the averaging interval.

Thus, we obtained the following main results for APBs.

1. The flexo-rotational effect induces an odd polarization distribution, which is more energy-beneficial than the even one.
2. At $T < T_S$, the flexo-rotational effect leads to the appearance of a spontaneous polarization in soft APBs, which are the most favorable energetically.
3. For the first time, we have derived an analytical solution for the dependence of the spontaneous polarization in a vicinity of APB on the temperature and the coefficients of flexoelectric coupling and rotostriction.
4. The calculated values of pyroelectric coefficient fall within the interval of typical values 10^{-4}–10^{-7} C/m^2/K [29], which allows the results of our theoretical calculations to be checked experimentally within the PyroSPM method.

4. Conclusions

The flexo-rotational effect can induce an improper spontaneous polarization and, as a consequence, a pyroelectric activity in a vicinity of the ferroelastic antiferrodistortive phase boundary in virtual ferroelectrics like $CaTiO_3$, $SrTiO_3$, and $EuTiO_3$. In $SrTiO_3$, the flexo-rotational effect induces a higher spontaneous polarization at much higher temperatures than those predicted earlier while considering other mechanisms of ferroelectric coupling. This result agrees with the experimental data [14], which were obtained but not explained ear-

T a b l e

Parameter	SI	Value
ε_b	dimensionless	43
α_T	10^6 m/(F·K)	0.75
$T_0^{(E)}$	K	30
$T_q^{(E)}$	K	54
a_{ij}	10^9 m^5/(C^2·F)	$a_{11}^u = 2.025$, $a_{12}^u = 1.215$, $a_{11}^\sigma = 0.820$, $a_{12}^\sigma = 1.396$
q_{ij}	10^{10} m/F	$q_{11} = 1.251$, $q_{12} = -0.108$, $q_{44} = 0.243$
Q_{ijkl}	m^4/C^2	$Q_{11} = 0.051$, $Q_{12} = -0.016$, $Q_{44} = 0.020$
g_{ijkl}	10^{-11} V·m^3/C	$g_{11} = g_{44} = 1$, $g_{12} = 0.5$
β_T	10^{26} J/(m^5·K)	9.1
T_S	K	105
$T_q^{(\Phi)}$	K	145
b_{ij}	10^{50} J/m^7	$b_{11}^u = 1.94$, $b_{12}^u = 3.96$. $b_{11}^\sigma = 0.93$, $b_{12}^\sigma = 3.88$
r_{ij}	10^{30} J/(m^5)	$r_{11} = 1.3$, $r_{12} = -2.5$, $r_{44} = -2.3$
R_{ij}	10^{19} m^{-2}	$R_{11} = 0.882$, $R_{12} = -0.777$, $R_{44} = -1.811$
η_{ijkl}	10^{29} (F·m)$^{-1}$	$\eta_{11}^u = -3.366$, $\eta_{12}^u = 0.135$, $\eta_{44}^u = 6.3$, $\eta_{11}^\sigma = -2.095$, $\eta_{12}^\sigma = -0.849$, $\eta_{44}^\sigma = 5.860$
v_{ijkl}	10^{10} J/m^3	$v_{11} = 0.28$, $v_{12} = -7.34$, $v_{44} = 7.11$
c_{ij}	10^{11} J/m^3	$c_{11} = 3.36$, $c_{12} = 1.07$, $c_{44} = 1.27$
s_{ij}	10^{-12} m^3/J	$s_{11} = 3.52$, $s_{12} = -0.85$, $s_{44} = 7.87$
F_{ijkl}	10^{-12} m^3/C	$F_{11} = -13.80$, $F_{12} = 6.66$, $F_{44} = 8.48$
Φ_S	radians	0.0235

F o o t n o t e: the superscripts u and σ denote coefficients for a constant deformation and a constant mechanical stress, respectively.

lier. Since this effect is possible for all crystal structures with statically tilted oxygen octahedra, the origin of the emergence of polarized subsurface layers in nonpolar substances becomes more clear.

APPENDICES

A. Material Parameters of Strontium Titanate Used in Numerical Calculations (see Table)

Parameter values were taken from works [11, 14, 19–24].

B. Temperature maximum of the pyroelectric coefficient

According to Eq. (16), the derivative of the polarization amplitude with respect to the temperature looks like

$$\Pi_3(T) \sim \frac{dp_0(T)}{dT} \sim -\frac{d}{dT}\left(\frac{\Phi_S^2}{l_\Phi}\right) \sim \frac{d}{dT}\left(b_1(T)\right)^{3/2}, \qquad \text{(D.1)}$$

since $\Phi_S^2(T) \sim -b_1(T)$, $l_\Phi(T) \sim \sqrt{-b_1^{-1}(T)}$, so that $\Phi_S^2/l_\Phi \sim (b_1(T))^{3/2}$. Using the dependence

$$b_i(T) = \beta_T T_q^{(\Phi)}\left(\coth\left(T_q^{(\Phi)}\Big/T\right) - \coth\left(T_q^{(\Phi)}\Big/T_S\right),\right)$$

we obtain

$$\Pi_3(T) \sim (b_1(T))^{1/2}\frac{db_1(T)}{dT} \sim \left(\frac{T_q^{(\Phi)}}{T}\right)^2 \times$$

$$\times \sinh^{-2}\left(\frac{T_q^{(\Phi)}}{T}\right)\sqrt{\coth\left(\frac{T_q^{(\Phi)}}{T}\right) - \coth\left(\frac{T_q^{(\Phi)}}{T_S}\right)}. \qquad \text{(D.2)}$$

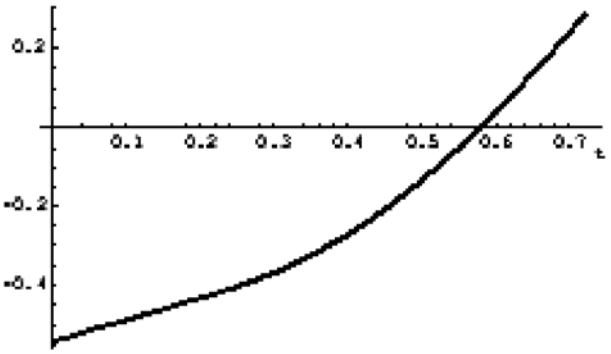

Fig. 5. Dependence of the left-hand side of Eq. (D.4) on the dimensionless temperature t

From formula (D.2), it is evident that $\Pi_3(T_S) = 0$ and $\Pi_3(0) = 0$. Let us introduce the dimensionless variables

$$\frac{T_q^{(\Phi)}}{T} = \frac{1}{t}, \quad \frac{T_q^{(\Phi)}}{T_S} = \frac{1}{t_S} = \frac{145}{105} \quad \text{(according to Table).} \qquad \text{(D.3)}$$

Then

$$\Pi_3(t) \sim \frac{1}{t^2\sinh^2(t)}\sqrt{\coth\left(\frac{1}{t}\right) - \coth\left(\frac{1}{t_S}\right)},$$

and the derivative $\frac{d\Pi_3(t)}{dt}$ equals zero, provided that

$$4\coth^2\left(\frac{1}{t}\right) + 4t\coth\left(\frac{1}{t_S}\right) - 4\coth\left(\frac{1}{t}\right) \times$$

$$\times\left(t + \coth\left(\frac{1}{t_S}\right)\right) + \cosh^{-2}\left(\frac{1}{t}\right) = 0. \qquad \text{(D.4)}$$

The numerical solution of this equation is $t = 0.58$ (see Fig. 5), i.e. the maximum of the pyroelectric coefficient is attained at a temperature of

$$0.58T_q^{(\Phi)} = 84.1 \text{ K}. \quad \text{(D.5)}$$

1. A. Ohtomo, D.A. Muller, J.L. Grazul, and H.Y. Hwang, Nature **419**, 378, (2002).
2. A. Ohtomo and H.Y. Hwang, Nature **427**, 423 (2004).
3. J.W. Park *et al.*, Nature Commun. **1**, 94 (2010).
4. J. Seidel *et al.*, Nature Mater. **8**, 229 (2009).
5. Ying-Hao Chu *et al.*, Nature Mater. **7**, 478 (2008).
6. S. J. May *et al.*, Nature Mater. **8**, 892 (2009).
7. M. Stengel, D. Vanderbilt, and N.A. Spaldin, Nature Mater. **8**, 392 (2009).
8. A. Vasudevarao *et al.*, Phys. Rev. Lett. **97**, 257602 (2006).
9. V. Gopalan and D.B. Litvin, Nature Mater. **10**, 376 (2011).
10. M.J. Haun, E. Furman, T.R. Halemane, and L.E. Cross, Ferroelectrics **99**, 55 (1989), ibidem p. 13.
11. A.K. Tagantsev, E. Courtens, and L. Arzel, Phys. Rev. B **64**, 224107 (2001).
12. B. Houchmanzadeh, J. Lajzerowicz, and E. Salje, J. Phys. Condens. Matter. **3**, 5163 (1991).
13. Sandra Van Aert, Stuart Turner, Rémi Delville, Dominique Schryvers, Gustaaf Van Tendeloo, and Ekhard K.H. Salje. DOI: 10.1002/adma.201103717.
14. P. Zubko, G. Catalan, A. Buckley, P.R.L. Welche, and J.F. Scott, Phys. Rev. Lett. **99**, 167601 (2007).
15. M.S. Majdoub, P. Sharma, and T. Cagin, Phys. Rev. B **77**, 125424 (2008).
16. G. Catalan, B. Noheda, J. McAneney, L.J. Sinnamon, and J.M. Gregg, Phys. Rev B **72**, 020102 (2005).
17. E.A. Eliseev, A.N. Morozovska, M.D. Glinchuk, and R. Blinc, Phys. Rev. B **79**, No. 16, 165433-1-10, (2009).
18. D. Lee *et al.*, Phys. Rev. Lett. **107**, 057602 (2011).
19. J.H. Barrett, Phys. Rev. **86**, 118 (1952).
20. P.A. Fleury and J.M. Worlock, Phys. Rev. **174**, 613 (1968).
21. Yijia Gu, Karin Rabe, Eric Bousquet, Venkatraman Gopalan, and Long-Qing, Chen. Phys. Rev. B **85**, 064117 (2012).
22. Rakesh K. Behera *et al.*, J. Phys. Condens. Matter. **23**, 175902 (2011).
23. A.N. Morozovska, E.A. Eliseev, M.D. Glinchuk, Long-Qing Chen, and Venkatraman Gopalan, Phys. Rev. B **85**, 094107 (2012).
24. A.N. Morozovska, E.A. Eliseev, S.V. Kalinin, Long-Qing Chen, and Venkatraman Gopalan, Appl. Phys. Lett. **100**, 142902 (2012).
25. J. Groten, M. Zirkl, G. Jakopic, A. Leitner, and B. Stadlober, Phys. Rev. B **82**, 054112 (2010).
26. A.N. Morozovska, E.A. Eliseev, S.L. Bravina, and S.V. Kalinin, Phys. Rev. B **75**, 174109 (2007).
27. N. Tayebi, Y. Narui, R.J. Chen, C.P. Collier, K.P. Giapis, and Y. Zhang, Appl. Phys. Lett. **93**, 103112 (2008).
28. S.V. Kalinin, A.N. Morozovska, L.Q. Chen, and B.J Rodriguez, Rep. Prog. Phys. **73**, 056502 (2010).
29. S.B. Lang, Phys. Today, **58**, No. 8, 31 (2005).
30. G. Rupprecht and R.O. Bell, Phys. Rev. **135**, A748 (1964).
31. G.A. Smolenskii, V.A. Bokov, V.A. Isupov, N.N Krainik, R.E. Pasynkov, and A.I. Sokolov, *Ferroelectrics and Related Materials* (Gordon and Breach, New York, 1984).
32. N.A. Pertsev, A.K. Tagantsev, and N. Setter, Phys. Rev. B **61**, R825 (2000).
33. J. Hlinka and P. Marton, Phys. Rev. B **74**, 104104 (2006).
34. W. Cao and R. Barsch, Phys. Rev. B **41**, 4334 (1990).
35. P. Zubko, G. Catalan, A. Buckley, P.R.L. Welche, and J.F. Scott, Phys. Rev. Lett. **99**, 167601 (2007).

Received 06.02.12.
Translated from Ukrainian by O.I. Voitenko

ПОЛЯРИЗАЦІЯ ТА ПІРОЕЛЕКТРИЧНИЙ КОЕФІЦІЄНТ В ОКОЛІ АНТИФЕРОДИСТОРСІЙНИХ ДОМЕННИХ ГРАНИЦЬ (НА ПРИКЛАДІ $SrTiO_3$)

Я.В. Яковенко, Є.А. Єлісєєв, С.В. Свєчніков, Г.М. Морозовська

Р е з ю м е

Із використанням теорії Ландау–Гінзбурга–Девоншира проведено аналітичні та чисельні дослідження просторових характеристик і температурних залежностей локальної поляризації і піроелектричного коефіцієнта в околі антиферодисторсійних фазових границь у $SrTiO_3$ при температурах, нижчих за температуру антиферодисторсійного структурного фазового переходу (≈ 105 K). Причиною поляризації пристіночної зони вважається флексоелектричний ефект і ротаційна стрикція (флексо-ротаційний ефект).